BIOCHEMISTRY

A direct heterotypic interaction between the DIX domains of Dishevelled and Axin mediates signaling to β-catenin

Kumpei Yamanishi[1]*, Marc Fiedler[2]*, Shin-ichi Terawaki[3], Yoshiki Higuchi[1†], Mariann Bienz[2†], Naoki Shibata[1†]

The Wnt–β-catenin signaling pathway regulates embryonic development and tissue homeostasis throughout the animal kingdom. Signaling through this pathway crucially depends on the opposing activities of two cytoplasmic multiprotein complexes: the Axin destruction complex, which destabilizes the downstream effector β-catenin, and the Dishevelled signalosome, which inactivates the Axin complex and thus enables β-catenin to accumulate and operate a transcriptional switch in the nucleus. These complexes are assembled by dynamic head-to-tail polymerization of the DIX domains of Axin or Dishevelled, respectively, which increases their avidity for signaling effectors. Axin also binds to Dishevelled through its DIX domain. Here, we report the crystal structure of the heterodimeric complex between the two DIX domains of Axin and Dishevelled. This heterotypic interface resembles the interfaces observed in the individual homopolymers, albeit exhibiting a slight rearrangement of electrostatic interactions and hydrogen bonds, consistent with the heterotypic interaction being favored over the homotypic Axin DIX interaction. Last, cell-based signaling assays showed that heterologous polymerizing domains functionally substituted for the DIX domain of Dishevelled provided that these Dishevelled chimeras retained a DIX head or tail surface capable of binding to Axin. These findings indicate that the interaction between Dishevelled and Axin through their DIX domains is crucial for signaling to β-catenin.

INTRODUCTION

The Wnt–β-catenin signaling cascade is ancient and mediates cell communication during development from the most primitive animals all the way to humans. It also controls stem cell function and regeneration of adult tissues, which may explain why its deregulation can cause cancer (*1*). In the absence of a Wnt signal, a multiprotein complex assembled by the scaffold protein Axin and the tumor suppressor adenomatous polyposis coli (APC) phosphorylates β-catenin through associated kinases [glycogen synthase kinase 3 (GSK3) and casein kinase 1α], thus targeting this key effector for ubiquitylation and proteasomal degradation (*2*). The activity of this Axin complex is blocked upon Wnt proteins binding to Frizzled receptors and to low-density lipoprotein receptor–related proteins 5 and 6 (LRP5/6) coreceptors, which triggers the assembly of a signalosome by the Frizzled-binding protein Dishevelled (*3*). Dishevelled thus recruits the Axin complex to LRP5/6 and stimulates the phosphorylation of specific motifs in the LRP5/6 intracellular tail that act as direct competitive inhibitors of GSK3 (*4*). Consequently, the phosphorylation of β-catenin by GSK3 is blocked, which enables β-catenin to accumulate and function as a transcriptional coactivator in the nucleus to operate a transcriptional switch (*5*).

Dishevelled and Axin each have a DIX domain, which, upon purification, undergoes reversible head-to-tail polymerization in vitro, as can be demonstrated by size exclusion chromatography or by analytical ultracentrifugation (*6*–*8*). This results in homopolymeric DIX domain filaments that can thus be observed by electron microscopy, or in protein crystals that have been used to determine the structure of the homodimeric interface in each case at high resolution (*6*, *8*, *9*). In cells, homopolymerization by these DIX domains manifests itself in the formation of discrete highly dynamic puncta, detectable by immunofluorescence, with the ability of Dishevelled to form puncta strictly correlating with its ability to signal (*10*). Structure-guided point mutations that block in vitro polymerization also block activity in vivo and were thus crucial to establish that the DIX-dependent polymerization of Axin and Dishevelled is essential for their functions in the destruction complex and in the Wnt signalosome, respectively (*6*, *7*, *11*). Furthermore, nuclear magnetic resonance (NMR) spectroscopy has demonstrated that the two DIX domains also use their head or tail surfaces to bind to each other (*7*). This led to the hypothesis that Dishevelled, once polymerized during Wnt signaling, copolymerizes with Axin to recruit it to the Wnt receptor complex at the cell surface and also to prevent it from assembling the destruction complex through homopolymerization (*7*, *12*). A corollary of this model is that the affinity of the DIX domain of Axin (herein to be called DAX) is higher for the DIX domain of Dishevelled (herein to be called DIX) than for itself, but this has not been tested. Furthermore, the interface between the two DIX domains has not been characterized at the atomic level.

Here, we determined the crystal structure of the complex between DIX and DAX at high resolution, which confirmed that the interaction between the two domains is mediated by the same key surface residues that also mediate the homotypic interactions, albeit with some of the electrostatic interactions and hydrogen bonds slightly rearranged. Furthermore, using fluorescence anisotropy to measure the dissociation constants (K_D) between individual domains, we established that the heterotypic DIX-DAX (and DAX-DIX) interaction is favored over the homotypic DAX-DAX interaction, consistent with the previously proposed copolymerization model (*7*, *12*).

[1]Department of Picobiology, Graduate School of Life Science, University of Hyogo, 3-2-1 Koto, Kamigori-cho, Ako-gun, Hyogo 678-1297, Japan. [2]Medical Research Council Laboratory of Molecular Biology, Francis Crick Avenue, Cambridge CB2 0QH, UK. [3]Graduate School of Science and Technology, Gunma University, 1-5-1 Tenjin-cho, Kiryu, Gunma 376-8515, Japan.
*These authors contributed equally to this work.
†Corresponding author. Email: shibach@sci.u-hyogo.ac.jp (N.S.); mb2@mrc-lmb.cam.ac.uk (M.B.); hig@sci.u-hyogo.ac.jp (Y.H.)

Last, we designed Dishevelled chimerae in which the DIX domain is replaced by heterologous polymerization domains to establish that the latter are inactive in cell-based signaling assays, although they are capable of assembling signalosome-like particles in the transfected cells. However, their signaling activities were restored by the addition of a single DIX head or tail surface that is capable of binding to DAX. This provides evidence that the head-to-tail interaction between DIX and DAX is important for signaling to β-catenin.

RESULTS

Structure determination of the heterotypic DAX-DIX complex

To obtain crystals of the DAX-DIX complex, we used a flexible peptide linker to fuse the C terminus of human AXIN1 DAX to the N terminus of human DVL2 DIX to enforce a defined 1:1 stoichiometry between the two domains, thereby avoiding random and heterogeneous heteropolymerization between them (Fig. 1A). In addition, we used the polymerization-deficient point mutants M4 in the head surface of DAX (Y760D) and M2 in the tail surface of DIX (V67A and K68A) to increase the solubility of these domains (Fig. 1B).

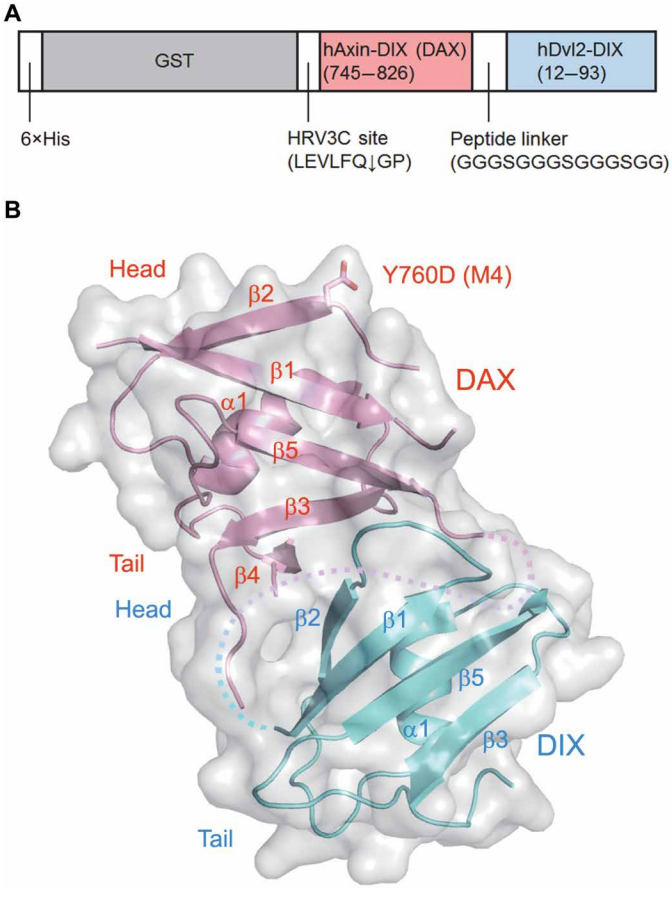

Fig. 1. Crystal structure of the DAX-DIX dimer. (**A**) Construct in which DVL2 DIX was fused to Axin DIX (DAX) downstream of a flexible linker. The His and GST tags were removed before crystallization by cleaving with the protease HRV3C. (**B**) Ribbon diagram and space-filling model of the DAX-DIX dimer. Pink, DAX; cyan, DIX; dotted line, flexible linker between DAX and DIX (not structured). The tail of DIX (including the M2 mutation) is not visible in the structure owing to poor electron density.

DAX-DIX crystals were obtained by microseeding, and x-ray diffraction data were integrated and scaled at 3.09 Å resolution in space group $P2_12_12$, exhibiting one heterodimer per asymmetric unit (table S1), and the structure of the heterodimer complex was solved by molecular replacement. The overall structures of DIX and DAX in the complex are essentially a ubiquitin fold with five β strands (β1 to β5) and one α helix as in their respective homotypic polymers, although the electron density for the tail region of DIX (residues 54 to 80) including the M2 mutation site on β4 was not strong enough to build coordinates for this C-terminal region (Fig. 1B). β4 of DAX and β2 of DIX form a parallel intermolecular bridge mainly composed of a hydrophobic cluster (site A) formed by Tyr^{787} and Phe^{801} of DAX and Tyr^{27} of DIX, as in the homotypic DIX-DIX and DAX-DAX interfaces (Fig. 2A) (*6*, *8*, *9*). However, the DIX-DIX interface comprises a second interaction site (site B) in which Asp^{61} and Asp^{63} in one molecule (Mol-1) form salt bridges with Arg^{84} of the other molecule (Mol-2) and Asp^{61} (Mol-1) forms a hydrogen bond with Asn^{82} (Mol-2), although neither the hydrophilic nor the electrostatic interaction was detected in the DAX-DIX and DAX-DAX interfaces (Fig. 2B). This may explain why the homotypic DIX-DIX affinity (K_D = 4.9 μM by fluorescence anisotropy; 5 to 20 μM by analytical ultracentrifugation) appears to be stronger than that of DAX-DAX (45 μM) or their heterotypic interaction (see below). Last, at the DAX-DIX interface, loop 1 (between β1 and β2) of DIX slightly shifts toward the interface of DAX, resulting in additional hydrogen bonds between Glu^{23}, Glu^{24}, and Thr^{25} of DIX and Lys^{789} and Lys^{821} of DAX (site C) (Fig. 2C). NMR spectroscopy also indicated that these residues are engaged in the heterotypic interaction (*7*), possibly contributing to the slightly increased affinity between DIX and DAX compared to that of the homotypic DAX-DAX interaction.

The overall structure of the DAX-DIX complex superimposes very well on those of the homotypic dimers, with root mean square deviations of 1.37 Å (to DIX dimer) and 0.92 Å (to DAX dimer) for the main chains. This suggests that DIX and DAX can form helical heteropolymers. However, the oligomerization of DAX-DIX did not elongate beyond the dimer in the crystal, probably because the point mutations in the DIX head surface and DAX tail surface weakened the DIX-DAX interaction necessary for polymer extension. However, a DIX-DAX heteropolymer can be modeled from DAX-DIX dimers by successive superimposition and exhibits a helical polymer with six monomers per turn with a width and pitch of ~71 and ~75 Å, respectively—almost identical to the structures observed for DIX and DAX homopolymers (fig. S1, A and B).

Binding affinities between DIX and DAX domains

Next, we used fluorescence anisotropy assays to estimate the K_D values for the homo- and heterotypic interactions between DIX and DAX (Fig. 3, A and B) (*13*). To avoid polymerization, we disabled the head surface of these domains with the M4 (Y27D in DIX) or M3 mutation (I758A and R761D in DAX), whereas the tail surface was disabled by the M2 mutation in both domains (V67A/K68A in DIX and V800A/F801A in DAX; Figs. 2 and 3) (*6*, *7*). We also included two double mutants, DIX-M2M4 (Y27D/V67A/K68A) and DAX-M2M3 (I758A/R761D/V800A/F801A), as negative controls. This allowed us to measure specifically the binding between the head surface of one domain with the tail surface of another.

The homotypic DIX-DIX interaction displayed the highest affinity with a K_D value of 4.9 μM, consistent with the reported value estimated by analytical ultracentrifugation (*6*). The K_D values of the heterotypic

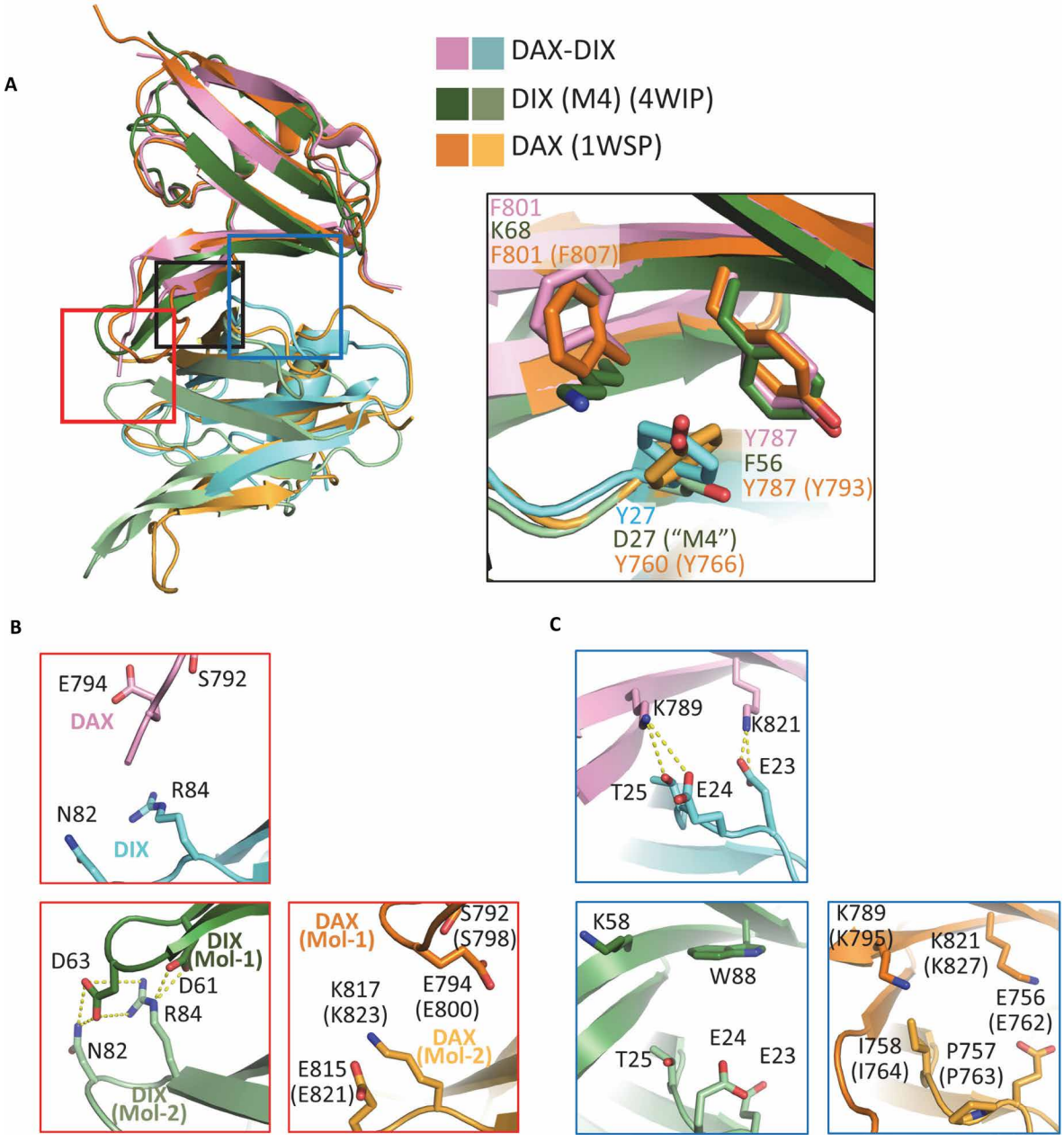

Fig. 2. Comparison of DAX-DIX, DIX-DIX, and DAX-DAX structures. (**A**) Superimposition of DAX-DIX heterodimer onto homodimers of DIX-DIX and DAX-DAX, as indicated in key. Rectangles highlight distinct interaction sites between DIX domains: black, site A (see also inset); red, site B; blue, site C. Amino acid numbering reflects the human proteins, including the DAX-DAX homodimer structure, which was solved using rat Axin (residue numbers for the rat protein are shown in parentheses). (**B** and **C**) Close-up views of site B (B) and site C (C). Dashed lines indicate salt bridges and hydrogen bonds.

interactions were 24 μM (DAX-M3 and DIX-M2) or 9 μM (DIX-M4 and DAX-M2), in each case statistically significantly higher than that of the homotypic DIX-DIX interaction (regardless of the mutant combination). In addition, these values are 6- to 22-fold lower than their respective double-mutant (M2M4 or M2M3) negative controls. Our results are consistent with previous work (*7*), although we suggest that the NMR titrations used to estimate the affinity between DIX-M2 and DAX-M3 likely underestimated the affinity of this heterotypic interaction, given that some small fraction of the ^{15}N-labeled protein tends to aggregate and does therefore not contribute to the signals from which the K_D values are derived. Note also that the concentration of the ^{15}N-labeled DAX-M3 (100 μM) used for the NMR titrations (*7*) is far higher than the concentration of fluorescently labeled DAX-M3 used here (0.5 μM), which approximates the normal cellular concentration of Axin in mammalian cells (~0.1 μM) (*14*). We could not completely disable the interaction surfaces by these point mutations, likely because these mutants retain their shape complementarity to some extent. However, these mutants do not form puncta in cells even when they are overexpressed (*6*, *7*), indicating that the concentrations of these mutants are lower than the K_D values. Last, the homotypic DAX-DAX interaction exhibited the highest K_D value (45 μM) of our series, indicating the weakest affinity (Fig. 3B). Note

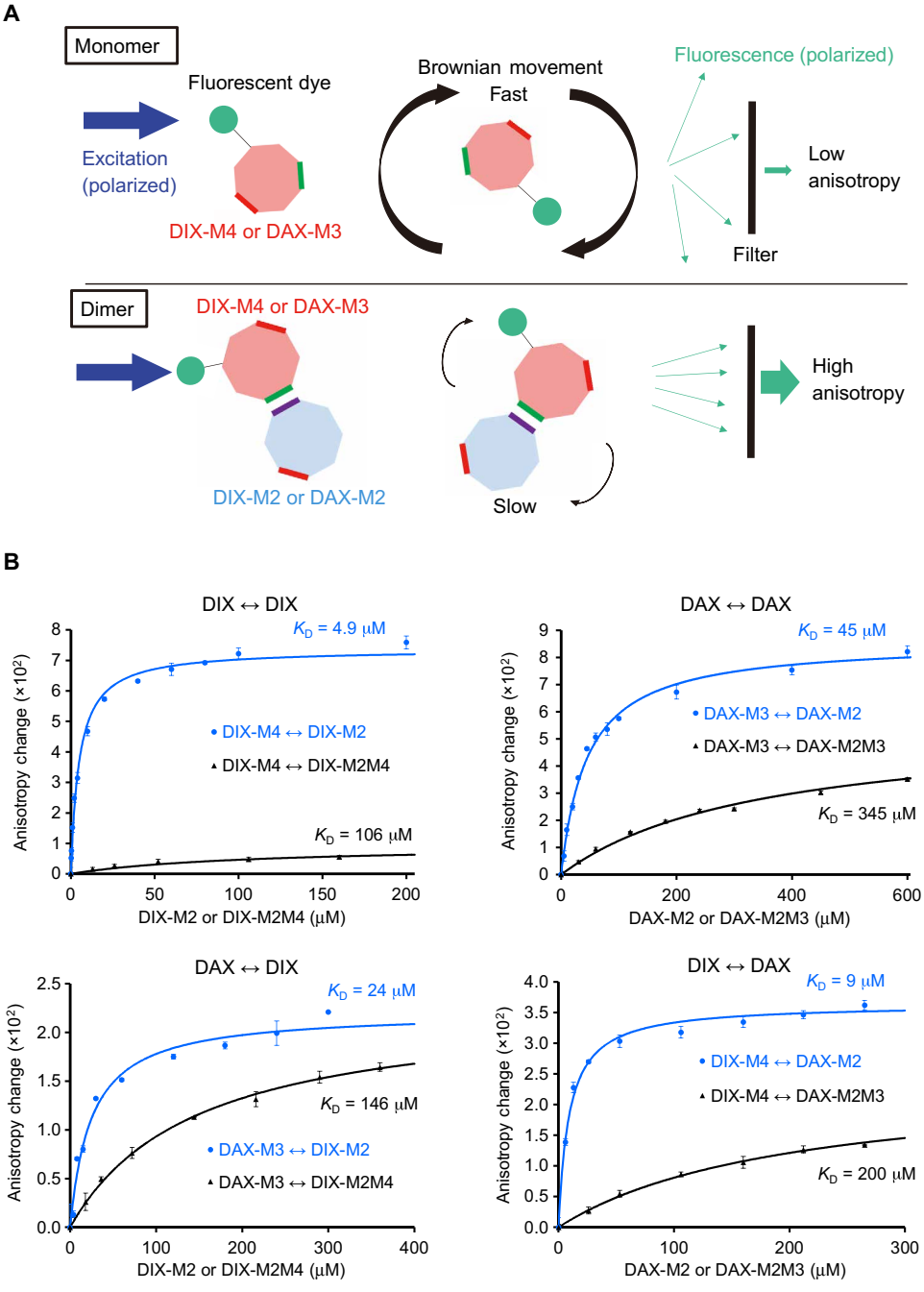

Fig. 3. Fluorescence anisotropy binding assays. (**A**) Effect of dimerization on the fluorescence anisotropy of labeled DIX domains. Fluorescence anisotropy correlates inversely with the rotational mobility of the fluorophores that are excited with polarized light. Assays tested whether an unlabeled DIX or DAX molecule (blue) reduced the mobility of a fluorophore-labeled DIX or DAX molecule (pink), as indicated by an increase in fluorescence anisotropy. The binding interfaces are indicated by colored bars: red bars, disabled head (M4 or M3) or tail (M2) surfaces; purple bars, intact head surfaces; green bars, intact tail surfaces. (**B**) Fluorescence anisotropy curves of the indicated labeled DIX and DAX proteins upon titration with unlabeled DAX and DIX, respectively. Data represent the mean ± SD. $n = 3$ independent experiments.

that all our measurements were based on mutant recombinant domains that may be less stable than the wild-type domains, and so, some of our K_D values could be underestimates. These side-by-side comparisons indicate that the affinity of the homotypic DAX-DAX interaction is about one order of magnitude lower than that of the DIX-DIX interaction, with that of the heterotypic DAX-DIX and DIX-DAX interactions being intermediate.

Requirement for the heterotypic DAX-DIX interaction in Wnt signal transduction to β-catenin

The signaling activity of Dishevelled is abolished by DIX mutations that block its polymerization (*6*, *7*, *11*). However, given that the mutated residues also engage in crucial contacts with DAX (Fig. 2), it is impossible to disentangle polymerization and Axin interaction by these mutations alone. In other words, there is no conclusive proof yet that the interaction between Dishevelled and Axin through their DIX domains is functionally relevant for signaling to β-catenin. Sequences outside their DIX domains might enhance their mutual interaction.

We thus asked whether we could substitute the DIX domain of Dishevelled with a heterologous polymerization domain and whether the latter could confer assembly of a functional signalosome. We chose the PB1 (Phox and Bem1) domain from the p62 autophagy receptor, a close structural relative of the DIX domain that forms helical filaments in vitro (*15*) and mediates the assembly of dynamic punctate structures in cells (*16*), or the SAM domain (sterile α motif) from tankyrase, the only known module that is structurally distinct from the DIX and PB1 domains that is capable of assembling head-to-tail polymers (*17*, *18*). DVL2 chimerae, in which the DIX domain was replaced with either of these domains (PB1-DVL2-ΔDIX and SAM-DVL2-ΔDIX; Fig. 4A), formed cytoplasmic puncta similar to wild-type DVL2 upon overexpression in COS-7 cells (Fig. 4B), indicating that these heterologous domains can mediate polymerization of Dishevelled in cells. However, when we tested the signaling activity of these DVL2 puncta-forming chimerae in DVL null-mutant human embryonic kidney (HEK) 293T cells (*11*), using a Wnt-specific luciferase reporter (SuperTOP) (*19*), we found that they were completely inactive (Fig. 4C). As expected from this, they did not colocalize with Axin (Fig. 4B), similarly to DVL2-ΔDIX itself (*10*), demonstrating that these chimerae were incapable of interacting with Axin despite polymerizing into signalosome-like structures.

We asked whether we could restore signaling activity in these chimerae by fusing them to a mutant DIX domain in which polymerization

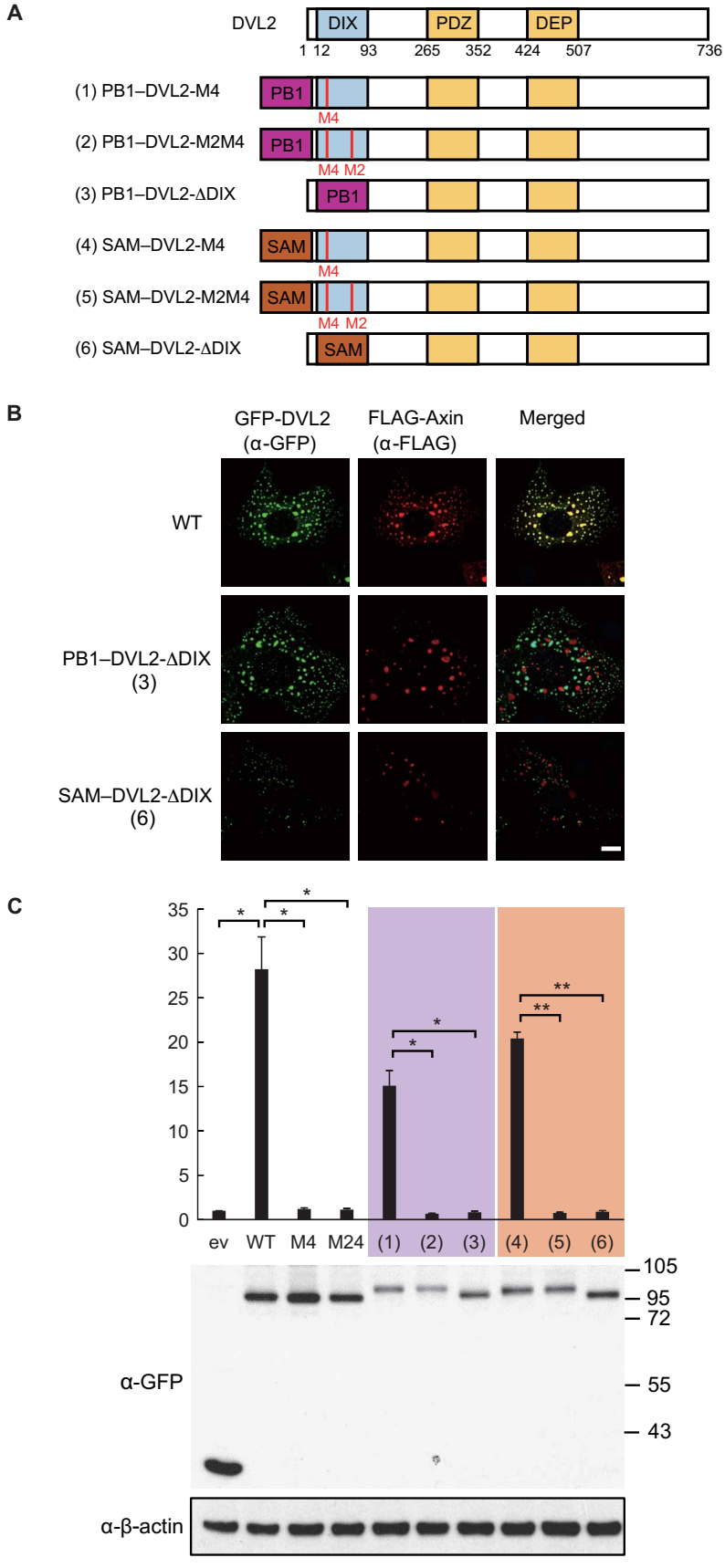

Fig. 4. Signaling by DVL2 chimerae. (**A**) Cartoons of GFP-tagged wild-type (WT) DVL2 and corresponding DVL2 chimerae bearing a PB1 or SAM domain in place of the DIX domain. Amino acid numbers in WT DVL2 denote domain boundaries. (**B**) Representative confocal images of COS-7 cells coexpressing FLAG-tagged Axin and WT GFP-DVL2 or GFP-DVL2 chimerae, fixed and stained as indicated above panels. Images of the other chimerae are presented in the Supplementary Materials (fig. S2). $n = 3$ independent experiments. Scale bar, 10 μm. (**C**) SuperTOP reporter assays monitoring signaling activities of WT, M2 or M2M4 mutant GFP-DVL2, and GFP-DVL2 chimerae 1 to 6 in DVL-null HEK293T cells. Fold induction levels relative to empty pEGFP vector control (ev) are shown. Data represent the mean ± SEM. Multiplicity adjusted: $^{*}P < 0.043$ and $^{**}P < 0.0043$, one-way ANOVA test. $n = 3$ independent experiments. Corresponding Western blots are shown to indicate comparable protein levels.

is disabled by an M4 head mutation but which retains a normal tail surface capable of binding to Axin or to a double-mutant domain whose interaction with Axin is compromised by mutations in both Axin-binding surfaces as a control (Fig. 4A). The single-mutant M4 DIX domain restored partial (>50%) signaling activity in both types of chimerae, whereas the chimerae bearing M2M4 double-mutant domains remained completely inactive (Fig. 4C). Likewise, partial colocalization with Axin was restored by M4 but not by M2M4 (fig. S2).

We also tested these chimerae in our complementation assay in which the signaling defect of DVL null-mutant HEK293T cells can be rescued by DVL2 constructs that are expressed stably at physiological concentrations (*11*). Whereas wild-type DVL2 exhibited Wnt-dependent signaling activity in this assay, neither M2M4 nor M4 mutant DVL2 did (fig. S3). In the case of the PB1 chimerae, only the M4 version showed statistically significant Wnt inducibility, but M2M4 did not (fig. S3). In contrast, both SAM chimerae showed Wnt-inducible activity, although this was significantly higher in the case of SAM M4 compared to SAM M2M4 (fig. S3). Note that these activities of the SAM chimerae may partly reflect an indirect interaction with Axin mediated by their polymerization with endogenous tankyrase (*17*, *18*). In conclusion, these results from the Wnt-dependent signaling assays are loosely consistent with those from the transient Dishevelled-dependent signaling assays (Fig. 4C) and support the notion that the heterotypic DIX-DAX interaction is important for the signaling of Dishevelled to β-catenin.

DISCUSSION

Here, we focused on the interaction between Axin and Dishevelled mediated by their DIX domains. We have solved the crystal structure of the DAX-DIX heterodimer, which provides a detailed map of the molecular architecture of the interface between the two proteins. It allowed us to establish that this heterotypic interaction between Axin and Dishevelled relies on the same key residues that also confer homotypic polymerization of the two DIX domains. Furthermore, the structural details of this interface help to explain why the affinity of the heterotypic DAX-DIX interaction appears intermediate between those of the homotypic

interactions, as determined in our study. Last, we used cell-based signaling assays based on Dishevelled chimerae in which polymerization relies on heterologous polymerization domains to show that a single DIX surface capable of binding to Axin was necessary and sufficient for Dishevelled signaling to β-catenin, although this remains to be shown conclusively in a physiological Wnt-dependent signaling context. Our results provide evidence for the functional importance of the DAX-DIX interface in mediating the interaction between Dishevelled and Axin, in addition to the separate functions of these domains in mediating homopolymerization of the two proteins.

Our affinity measurements indicated that the DIX-DIX interaction is about one order of magnitude stronger than the DAX-DAX interaction, with the heterotypic DAX-DIX and DIX-DAX interactions being intermediate. Thus, the heterotypic interactions appear to be favored over DAX-DAX interactions, whose low self-affinity in the Axin polymer render them vulnerable to disruption by Dishevelled DIX, especially at high local concentrations of DIX after polymerization. This supports the hypothesis of a two-pronged inhibition of the Axin complex by Dishevelled, as previously proposed (*7*, *12*): Polymerized Dishevelled not only recruits the Axin complex to the Wnt receptor complex upon its binding to Wnt, to bring its associated GSK3 kinase into proximity of the phosphorylated tail of the LRP5/6 coreceptor for direct inhibition, but also breaks up Axin-DAX polymers that are critical for the function of the β-catenin destruction complex. Direct evidence supporting this breakup of Axin polymers by Dishevelled comes from the observation that the recruitment of Axin into Dishevelled signalosomes destabilizes Axin protein assemblies by increasing their dynamicity, as measured by photobleaching experiments (*10*). Our results with the Dishevelled chimerae provide evidence that a single functional DIX surface can suffice to confer signaling activity, and so, it is possible that the capturing of individual DAX domains at the end of short DIX filaments underlies both inhibitory activities. It is also conceivable that individual DAX domains are integrated into DIX filaments through copolymerization, but because these filaments are highly dynamic and expected to rearrange rapidly, without a fixed structure, the two modes of possible interactions—end-addition and copolymerization—could occur simultaneously and blend into one another.

Wnt signalosomes are apparently phase-separated dynamic protein complexes assembled by the Dishevelled hub protein in two steps (*10*, *20*), namely, by head-to-tail polymerization of its DIX domain followed by cross-linking of the DIX polymers by its DEP domain that undergoes domain swapping (*21*). Our study shows that the DIX domain–dependent polymerization can be functionally substituted by heterologous polymerizing domains, including the structurally unrelated SAM domain. This underscores the notion of head-to-tail polymerization as a general molecular principle underlying phase separation in physiologically relevant protein complexes such as signalosomes, although other molecular features have been implicated in the formation of distinct classes of phase-separating biological condensates, including multivalent protein interactions involving protein domains and their cognate unstructured motifs (*22*). It is remarkable that, in the case of Dishevelled, the homopolymerizing module also harbors the interacting surface for its key signaling effector Axin, and our work has shown that these two functions can be separated without loss of signaling function. This illustrates an example of an elegantly simple and parsimonious design principle wherein the assembly function and effector interaction reside within the same protein domain.

MATERIALS AND METHODS

Plasmids

For crystallization of DAX-DIX, a synthetic DNA, codon-optimized for *Escherichia coli* expression by GeneArt GeneOptimizer (Thermo Fisher Scientific), expressing a fusion protein of DAX (human Axin, residues 745 to 826) and DIX (human DVL2, residues 12 to 93) connected by a peptide linker (GGGSGGGSGGGSGG) was subcloned into plasmid pCold-GST (glutathione *S*-transferase) vector (Takara Bio). Point mutations at the interaction interface, namely, Y760D (M4) in DAX and V67A/K68A (M2) in DIX, were generated by polymerase chain reaction (PCR). For signaling assays and immunofluorescence staining, wild-type and mutant human DVL2, and human Axin were subcloned into pEGFP and pCMV-tag2B vectors, respectively. DVL2 DIX was also substituted with PB1 (human Sequestosome-1, residues 2 to 102) or SAM (human Tankyrase-2, residues 873 to 936) by PCR. For fluorescence anisotropy measurements, the DIX and DAX mutants were subcloned into pCold-GST and pCold I vectors (Takara Bio), respectively.

Expression, purification, and crystallization of DAX-DIX

The DAX-DIX dimer was expressed in *E. coli* BL21-CodonPlus(DE3)-RP (Agilent Technologies). The cells were cultured at 37°C while shaking them in 9 liters of LB media with chloramphenicol (30 μg/ml) and ampicillin (100 μg/ml). When OD_{600nm} (optical density at 600 nm) reached 0.5, expression of the recombinant protein was induced by adding isopropyl-β-D-thiogalactopyranoside (IPTG) to the culture at a final concentration of 0.3 mM followed by incubation overnight at 15°C with shaking. The cells were harvested by centrifugation at 10,000*g* for 5 min at 4°C.

Cells were resuspended with phosphate-buffered saline (PBS) containing 0.1% Triton X-100, 1 mM EDTA, 1 mM phenylmethylsulfonyl fluoride, and 1 mM dithiothreitol (DTT) and then disrupted by sonication. Cell lysates were cleared by centrifugation at 23,000*g* and then applied onto 25 ml of COSMOGEL GST-Accept (Nacalai Tesque). The column was washed with HRV3C protease buffer containing 10 mM Hepes buffer (pH 7.4), 150 mM NaCl, and 1 mM DTT. DAX-DIX was then cleaved off from the 6×His-GST tag bound to the resin by adding HRV3C protease and incubating overnight at 4°C. Protease-treated protein was applied onto a column containing COSMOGEL His-Accept (Nacalai Tesque) to remove contaminating uncleaved protein and 6×His-GST tag. Flow-through fractions were concentrated with Amicon (Merck KGaA) and applied onto a HiLoad 26/60 column (GE Healthcare). The eluted fractions containing DAX-DIX were collected and concentrated.

Purified protein was concentrated to 10 mg/ml, and tris(2-carboxyethyl)phosphine hydrochloride (pH 9.0) was added at a final concentration of 10 mM. Crystallization screening was performed by sitting drop vapor diffusion in 96-well plates (Greiner). The following screening kits were used: Wizard I, II, III, and IV and Precipitant Synergy (Rigaku Reagents); PEGRx 1 and 2 and PEG/Ion 1 and 2 (Hampton Research); and ProPlex, PGA Screen, and MIDAS (Molecular Dimensions). Initially, we obtained crystals from PEGRx 2 #18 containing 10% (v/v) 2-propanol, 0.1 M bicine (pH 8.5), and 30% (w/v) PEG1500 (polyethylene glycol, molecular weight 1500). Crystals were ground with a glass stick and suspended in fresh reservoir solution (seed stock). In the final crystallization setup, 0.5 μl of the purified protein was mixed with 0.4 μl of PACT premier #B4 [25% (w/v) PEG1500 and 0.1 M malonate-imidazole-borate (MIB) buffer (pH 7.0)] and 0.1 μl of the seed stock.

X-ray diffraction and data processing

X-ray diffraction of DAX-DIX crystals was performed at BL44XU, SPring-8 (Hyogo, Japan). Before cryo-cooling crystals in liquid nitrogen, crystals were soaked briefly in a cryo-protectant solution containing 30% (w/v) PEG1500, 0.1 M MIB buffer (pH 7.0), and 20% (v/v) glycerol. Crystals were cryo-cooled in a 100 K stream of cryogenic nitrogen gas during data collection. Data were indexed, integrated, and scaled with the program XDS (*23*).

Structure determination and refinement

The structure of DAX-DIX was solved by molecular replacement, based on the structures of Axin-DIX (*6*) and M4-mutant DVL2-DIX (*9*), as templates for the DAX and DIX parts, respectively. Structure refinement and manual model building were performed with PHENIX (*24*) and COOT (*25*). Color figures were prepared with PyMOL (*26*).

Cell culture and transfections

DVL null-mutant HEK293T cells (*11*) were used for all signaling assays and COS-7 cells (obtained from the American Type Culture Collection) for immunofluorescence. Cells were grown in Dulbecco's modified Eagle's medium (Life Technologies) containing 10% fetal calf serum and 1% penicillin-streptomycin. Transfection of cells was performed in Opti-MEM (Thermo Fisher Scientific) containing 100 to 400 ng of plasmid DNA per six-well plate with polyethylenimine (PEI) at a 1:3 ratio of DNA:PEI when cells were 40 to 60% confluent. After 4 hours, transfections were stopped by switching to normal Opti-MEM. Twenty hours later, cells were fixed with PBS containing 4% paraformaldehyde for immunofluorescence staining, or cell lysates were prepared for SuperTOP luciferase assays. Complementation assays were essentially performed as described, with or without stimulation with Wnt3a-conditioned medium for 6 hours (*11*).

SuperTOP luciferase reporter assays

Measurements of β-catenin–dependent transcription were performed using Dual-Luciferase Reporter Assay (Promega Corporation). Plasmid pSuperTOP, containing TCF/LEF (T cell factor/lymphoid enhancer-binding factor) sites upstream of a firefly luciferase reporter, and control *Renilla* luciferase in pRL were transfected in addition to pEGFP-DVL2 and pCMV-Axin. Cells were lysed with 500 μl of passive lysis buffer (Promega) per six-well plate, and cell debris was separated by centrifugation. Ten microliters of supernatant was dispensed into a Costar 96-well assay plate (Corning), and luciferase assay substrate was added as instructed by the manufacturer (Promega). Firefly luciferase activity was measured with an Orion microplate luminometer (Novara), reactions were stopped by adding stop reagent, and *Renilla* luciferase activity was measured subsequently. For each sample, firefly luciferase activity was divided by *Renilla* luciferase activity, and β-catenin–dependent transcription is shown as fold change relative to empty pEGFP vector (Fig. 4C) or DVL2 M2M4 cells (fig. S3). Assays from three (Fig. 4C) or seven (fig. S3) independent experiments were performed, statistical significance was assessed by repeated-measures one-way analysis of variance (ANOVA) followed by a Tukey's multiple comparison test, and the data are shown as means ± SEM with multiplicity-adjusted *P* values.

Immunofluorescence staining

EGFP-DVL2 constructs (100 ng) and FLAG-Axin (300 ng) per six-well plate were cotransfected with Lipofectamine 2000 (Invitrogen), fixed, permeabilized, and stained 20 hours later with rabbit anti-GFP (green fluorescent protein) (G1544, Sigma) and mouse anti-FLAG antibody (F1804, Sigma), followed by Alexa Fluor 488–conjugated goat anti-rabbit (A11008, Invitrogen) and Alexa Fluor 594–conjugated goat anti-mouse secondary antibody (A11032, Invitrogen). COS-7 cells were then mounted in, and stained by, VECTASHIELD with 4′,6-diamidino-2-phenylindole (DAPI) and analyzed by confocal microscopy.

Fluorescence anisotropy

M2, M4, and M2M4 mutants of DVL2-DIX (residues 12 to 93) and M2, I758A/R761D/C754S/C797S (M3/C754S/C797S), and M2M3 mutants of Axin-DAX (residues 744 to 826) were expressed as 6×His-GST–tagged and 6×His-tagged proteins, respectively, and prepared similarly as DAX-DIX except that COSMOGEL His-Accept was used for purification of the DAX mutants. Purified DIX-M4 was then concentrated to 0.2 μM and labeled at Cys^{80} with 5-iodoacetamide fluorescein (5-IAF) (Sigma-Aldrich). Labeled 5-IAF is unlikely to block the interaction with unlabeled DIX because Cys^{80} is located >15 Å away (further than the size of 5-IAF) from either the head or tail surface of DIX. Purified DAX-M2 (1 to 400 μM) was titrated, and fluorescence emission at 520 nm was measured with an excitation wavelength of 491 nm. Likewise, for 0.2 μM of purified DAX-M3/C754S/C797S labeled with 5-IAF at Cys^{744}, 1 to 400 μM of DIX-M2 were titrated, and the fluorescence emission was measured with a spectrophotometer (FP-6500, JASCO Corporation, Japan). To measure homotypic interactions, the same samples were used, albeit in different combinations (DIX-M4 and DIX-M2; DAX-M3/C754S/C797S and DAX-M2/C754S/C797S). Twenty individual fluorescence anisotropy measurements were made for each sample, and averaged fluorescence anisotropy values were plotted against the concentration of unlabeled molecules. Curves were fit using Eqs. 1 and 2 (*27*), where $[L]_0$ and $[L]$ are the initial and final concentrations of molecules labeled with fluorescence dye; $[U]_0$ and $[U]$ are the initial and final concentrations of unlabeled molecules; $[LU]$ is the concentration of the complex; r_{min}, r_{max}, and R are minimum (fully dissociated), maximum (fully bound), and measured anisotropy; and K_D is the dissociation constant.

$$R = \frac{[L]}{[L]_0} r_{min} + \frac{[LU]}{[L]_0} r_{max} = \frac{[L]_0 - [LU]}{[L]_0} r_{min} + \frac{[LU]}{[L]_0} r_{max} \quad (1)$$

$$K_D = \frac{[L][U]}{[LU]} = \frac{([L]_0 - [LU])([U]_0 - [LU])}{[LU]} \quad (2)$$

SUPPLEMENTARY MATERIALS

stke.sciencemag.org/cgi/content/full/12/611/eaaw5505/DC1

Fig. S1. Models of DAX-DIX polymers based on the dimer structure.

Fig. S2. Colocalization between coexpressed FLAG-Axin and GFP-DVL2 chimerae bearing PB1 or SAM domains.

Fig. S3. Complementation of DVL-null cells by GFP-DVL2 chimerae stably expressed at physiological levels.

Table S1. Data collection and refinement statistics for DAX-DIX dimer.

View/request a protocol for this paper from *Bio-protocol*.

REFERENCES AND NOTES

1. R. Nusse, H. Clevers, Wnt/β-catenin signaling, disease, and emerging therapeutic modalities. *Cell* **169**, 985–999 (2017).
2. J. L. Stamos, W. I. Weis, The β-catenin destruction complex. *Cold Spring Harb. Perspect. Biol.* **5**, a007898 (2013).
3. J. Bilic, Y. L. Huang, G. Davidson, T. Zimmermann, C. M. Cruciat, M. Bienz, C. Niehrs, Wnt induces LRP6 signalosomes and promotes dishevelled-dependent LRP6 phosphorylation. *Science* **316**, 1619–1622 (2007).

4. J. L. Stamos, M. L. Chu, M. D. Enos, N. Shah, W. I. Weis, Structural basis of GSK-3 inhibition by N-terminal phosphorylation and by the Wnt receptor LRP6. *ELife* **3**, e01998 (2014).
5. M. Gammons, M. Bienz, Multiprotein complexes governing Wnt signal transduction. *Curr. Opin. Cell Biol.* **51**, 42–49 (2018).
6. T. Schwarz-Romond, M. Fiedler, N. Shibata, P. J. Butler, A. Kikuchi, Y. Higuchi, M. Bienz, The DIX domain of Dishevelled confers Wnt signaling by dynamic polymerization. *Nat. Struct. Mol. Biol.* **14**, 484–492 (2007).
7. M. Fiedler, C. Mendoza-Topaz, T. J. Rutherford, J. Mieszczanek, M. Bienz, Dishevelled interacts with the DIX domain polymerization interface of Axin to interfere with its function in down-regulating β-catenin. *Proc. Natl. Acad. Sci. U.S.A.* **108**, 1937–1942 (2011).
8. Y. T. Liu, Q. J. Dan, J. Wang, Y. Feng, L. Chen, J. Liang, Q. Li, S. C. Lin, Z. X. Wang, J. W. Wu, Molecular basis of Wnt activation via the DIX domain protein Ccd1. *J. Biol. Chem.* **286**, 8597–8608 (2011).
9. J. Madrzak, M. Fiedler, C. M. Johnson, R. Ewan, A. Knebel, M. Bienz, J. W. Chin, Ubiquitination of the Dishevelled DIX domain blocks its head-to-tail polymerization. *Nat. Commun.* **6**, 6718 (2015).
10. T. Schwarz-Romond, C. Merrifield, B. J. Nichols, M. Bienz, The Wnt signalling effector Dishevelled forms dynamic protein assemblies rather than stable associations with cytoplasmic vesicles. *J. Cell Sci.* **118**, 5269–5277 (2005).
11. M. V. Gammons, T. J. Rutherford, Z. Steinhart, S. Angers, M. Bienz, Essential role of the Dishevelled DEP domain in a Wnt-dependent human-cell-based complementation assay. *J. Cell Sci.* **129**, 3892–3902 (2016).
12. M. Bienz, Signalosome assembly by domains undergoing dynamic head-to-tail polymerization. *Trends Biochem. Sci.* **39**, 487–495 (2014).
13. N. Tanaka, A. R. Fersht, Identification of substrate binding site of GroEL minichaperone in solution. *J. Mol. Biol.* **292**, 173–180 (1999).
14. C. W. Tan, B. S. Gardiner, Y. Hirokawa, M. J. Layton, D. W. Smith, A. W. Burgess, Wnt signalling pathway parameters for mammalian cells. *PLOS ONE* **7**, e31882 (2012).
15. R. Ciuffa, T. Lamark, A. K. Tarafder, A. Guesdon, S. Rybina, W. J. Hagen, T. Johansen, C. Sachse, The selective autophagy receptor p62 forms a flexible filamentous helical scaffold. *Cell Rep.* **11**, 748–758 (2015).
16. G. Matsumoto, K. Wada, M. Okuno, M. Kurosawa, N. Nukina, Serine 403 phosphorylation of p62/SQSTM1 regulates selective autophagic clearance of ubiquitinated proteins. *Mol. Cell* **44**, 279–289 (2011).
17. L. Mariotti, C. M. Templeton, M. Ranes, P. Paracuellos, N. Cronin, F. Beuron, E. Morris, S. Guettler, Tankyrase requires SAM domain-dependent polymerization to support Wnt-β-catenin signaling. *Mol. Cell* **63**, 498–513 (2016).
18. A. A. Riccio, M. McCauley, M. F. Langelier, J. M. Pascal, Tankyrase sterile α motif domain polymerization is required for its role in wnt signaling. *Structure* **24**, 1573–1581 (2016).
19. M. T. Veeman, D. C. Slusarski, A. Kaykas, S. H. Louie, R. T. Moon, Zebrafish prickle, a modulator of noncanonical Wnt/Fz signaling, regulates gastrulation movements. *Curr. Biol.* **13**, 680–685 (2003).
20. R. P. Sear, Phase separation of equilibrium polymers of proteins in living cells. *Faraday Discuss* **139**, 21–34 (2008).
21. M. V. Gammons, M. Renko, C. M. Johnson, T. J. Rutherford, M. Bienz, Wnt signalosome assembly by DEP domain swapping of dishevelled. *Mol. Cell* **64**, 92–104 (2016).
22. S. F. Banani, H. O. Lee, A. A. Hyman, M. K. Rosen, Biomolecular condensates: Organizers of cellular biochemistry. *Nat. Rev. Mol. Cell Biol.* **18**, 285–298 (2017).
23. W. Kabsch, XDS. *Acta Crystallogr. D Biol. Crystallogr.* **66**, 125–132 (2010).
24. P. D. Adams, P. V. Afonine, G. Bunkoczi, V. B. Chen, I. W. Davis, N. Echols, J. J. Headd, L. W. Hung, G. J. Kapral, R. W. Grosse-Kunstleve, A. J. McCoy, N. W. Moriarty, R. Oeffner, R. J. Read, D. C. Richardson, J. S. Richardson, T. C. Terwilliger, P. H. Zwart, PHENIX: A comprehensive Python-based system for macromolecular structure solution. *Acta Crystallogr. D Biol. Crystallogr.* **66**, 213–221 (2010).
25. P. Emsley, B. Lohkamp, W. G. Scott, K. Cowtan, Features and development of Coot. *Acta Crystallogr. D Biol. Crystallogr.* **66**, 486–501 (2010).
26. Schrödinger LLC, The PyMOL molecular graphics system, version 1.8.
27. J. R. Lakowicz, *Principles of Fluorescence Spectroscopy* (Springer ed. 3, 2006), pp. 353–382.

Acknowledgments: We thank M. Gammons for technical advice and discussions and G. Leday for checking the statistics of Fig. 4C and fig. S3. Synchrotron radiation experiments were performed at SPring-8 with the approval of the Japan Synchrotron Radiation Research Institute (proposal nos. 2014A1035 and 2017A2538) and under the Cooperative Research Program of Institute for Protein Research, Osaka University (2017A6723 and 2017B6723) and at Photon Factory (2015R-66 and 2017G012). **Funding:** This research was supported by a Grant-in-Aid from Scientific Research on Innovative Areas for "Structural Cell Biology" from the Ministry of Education, Culture, Sports, Science and Technology (MEXT) (23121526 and 25121731 to N.S. and 23121527 and 25121705 to S.T.); by Hyogo Science and Technology Association to N.S.; by the Platform Project for Supporting in Drug Discovery and Life Science Research (Platform for Drug Discovery, Informatics, and Structural Life Science) from the Ministry of Education, Culture, Sports, Science and Technology (MEXT) to N.S.; by the Japan Agency for Medical Research and Development (AMED) to N.S.; by Cancer Research UK (C7379/A24639 to M.B.); and by the Medical Research Council (U105192713 to M.B.), **Author contributions:** K.Y., N.S., and S.T. constructed bacterial expression systems for DAX-DIX. K.Y. and N.S. performed purification, crystallization, and structural analysis of DAX-DIX. Y.H. directed the structural analysis of DAX-DIX. K.Y. and M.F. carried out immunofluorescence and Wnt signaling assays. M.B. directed the cell-based assays. K.Y., N.S., M.F., M.B., and Y.H. wrote the manuscript. **Competing interests:** The authors declare that they have no competing interests. **Data and materials availability:** Atomic models have been deposited in the Protein Data Bank with accession number 6JCK. All other data needed to evaluate the conclusions in the paper are present in the paper or the Supplementary Materials.

Submitted 29 January 2019
Accepted 14 November 2019
Published 10 December 2019
10.1126/scisignal.aaw5505

Citation: K. Yamanishi, M. Fiedler, S. Terawaki, Y. Higuchi, M. Bienz, N. Shibata, A direct heterotypic interaction between the DIX domains of Dishevelled and Axin mediates signaling to β-catenin. *Sci. Signal.* **12**, eaaw5505 (2019).

Science Signaling

A direct heterotypic interaction between the DIX domains of Dishevelled and Axin mediates signaling to β-catenin

Kumpei Yamanishi, Marc Fiedler, Shin-ichi Terawaki, Yoshiki Higuchi, Mariann Bienz and Naoki Shibata

Sci. Signal. **12** (611), eaaw5505.
DOI: 10.1126/scisignal.aaw5505

DIX domains drive Wnt–β-catenin signaling

Dishevelled (Dvl) stimulates Wnt–β-catenin signaling by recruiting Axin, a component of the β-catenin destruction complex, to the Wnt signalosome, thus stabilizing β-catenin. Both Dvl-mediated activation and Axin-mediated repression of signaling require homopolymerization through the DIX domains of each protein. Through structural analysis and biochemical assays with the DIX domain of human Dvl and the DIX domain of human Axin (DAX), Yamanishi *et al*. found that the heterotypic interface between DIX and DAX resembled the interfaces observed in the individual homopolymers and that DIX-DAX heteropolymerization was favored over DAX-DAX homopolymerization. These findings support a model in which Dvl-Axin heterodimerization, mediated by DIX domains, drives the recruitment of Axin to the Wnt signalosome and disruption of the β-catenin destruction complex.